annalen der physik
www.ann-phys.org

# Free-Electron Tomography of Few-Cycle Optical Waveforms

*Yuya Morimoto,* Bo-Han Chen, and Peter Baum**

**Ultrashort light pulses are ubiquitous in modern research but the electromagnetic field of the optical cycles is usually not easy to obtain as a function of time. Field-resolved pulse characterization requires either a nonlinear-optical process or auxiliary sampling pulses that are shorter than the waveform under investigation and pulse metrology without at least one of these two prerequisites is often thought to be impossible. Here is reported how the optical field cycles of laser pulses can be characterized with field-linear sensitivity and no ultrashort probe events. A free-space electron beam is let to cross with the waveform of interest. Randomly arriving electrons interact by means of their elementary charge with the optical waveform in a linear-optical way and reveal the optical cycles as the turning points in a time-integrated deflection histogram. The sensitivity is only limited by the electron-beam emittance and can reach the level of thermal radiation and vacuum fluctuations. Besides overturning a common belief in optical pulse metrology, the idea also provides practical perspectives for in situ characterization and optimization of optical waveforms in higher-harmonics experiments, ultrafast transmission electron microscopes, laser-driven particle accelerators, free-electron lasers, or generally any experiments with waveform-controlled laser pulses in a vacuum environment.**

## 1. Introduction

Ultrashort light pulses with a controlled electromagnetic waveform are central to modern research, because such pulses provide access to the time-dependent response of complex materials on the level of a single cycle of light with a time resolution of attoseconds or less.[1,2] For example, few-cycle pulses can control chemical reactions[3] and photoionization processes,[4] produce high-order harmonic radiation,[5–9] trigger electron emission from nanostructures,[10–12] shape free-electron beams into attosecond pulses,[13,14] steer and visualize field-induced currents in complex materials,[15–17] and accelerate particles with laser light.[18,19] Also, a substantial amount of energy can be concentrated into a subcycle time interval, providing unprecedented field strengths and intensities for rapid material processing or high-field experiments.[18,19]

Essential for almost all such experiments with few-cycle light is a profound knowledge of the electromagnetic waveform in space and time, in order to relate the measured observables to the forces that produce them. It is a common belief in optics that almost any pulse characterization method requires either a nonlinear-optical process or a probe pulse of even shorter duration than the pulse to be determined, or both. For example, pulse characterization techniques like intensity autocorrelation,[20] frequency-resolved optical gating,[21,22] spectral phase interferometry for direct electric-field reconstruction,[23] or dispersion-scan[24] rely on a nonlinear-optical effect such as second-harmonic generation, difference frequency mixing, higher-order harmonic generation, or optical-parametric conversion. Methods like electro-optic sampling,[25,26] photoelectron streaking,[27,28] petahertz nonlinear optical mixing,[29] all-optical cathode-ray oscilloscopes,[30–34] or direct-current metrology in optoelectronic device[35,36] are all based on test pulses or controllable events that are as short or shorter than the field cycles of interest. Linear-optical methods only provide relative quantities with respect to reference light, for example, with spectral interferometry.[37,38] Consequently, it is a widespread notion in ultrafast optics that a purely linear characterization of the electromagnetic field of a light wave with long probe pulses may be impossible, or at least unrealistic.

## 2. Free-Electron Tomography of Optical Waveforms

Here, we show how an optical waveform can be determined by neither using a nonlinear interaction nor an ultrashort sampling process. The idea is based on the use of free electrons instead of

Y. Morimoto
Ultrashort Electron Beam Science RIKEN Hakubi Research Team
RIKEN Cluster for Pioneering Research (CPR)
RIKEN Center for Advanced Photonics (RAP)
Wako 351-0198, Japan
E-mail: yuya.morimoto@riken.jp
P. Baum
Institute of Photonics Technologies (IPT)
University of Konstanz
Universitätsstraße 10, 78457 Konstanz, Germany
E-mail: peter.baum@uni-konstanz.de
B.-H. Chen[+]
National Tsing Hua University
Hsinchu 30013, Taiwan

The ORCID identification number(s) for the author(s) of this article can be found under https://doi.org/10.1002/andp.202200193

[+]Present address: Institute of Photonics Technologies (IPT) 101 Section 2, Kuang-Fu Road, Hsinchu 300044, Taiwan



**DOI: 10.1002/andp.202200193**

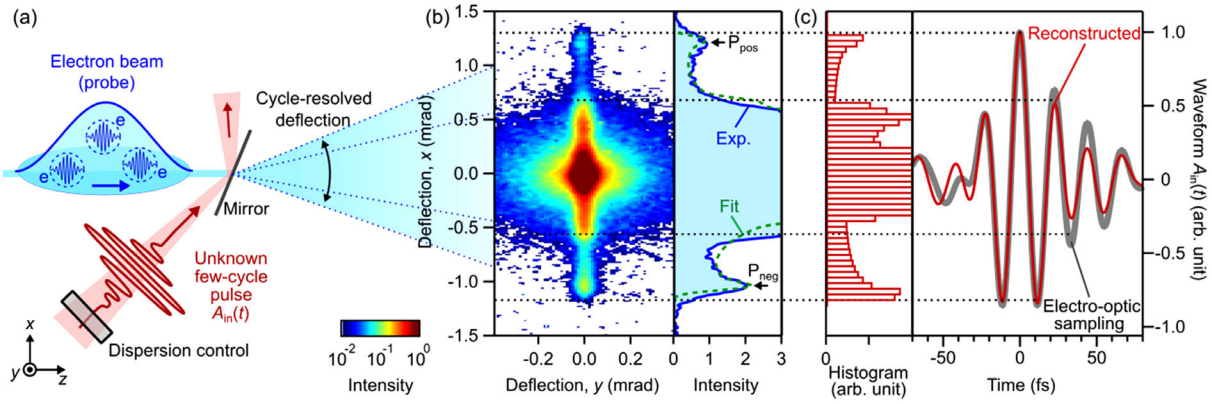


**Figure 1.** Concept and experiment for the linear-optical electron tomography of few-cycle waveforms. a) An electron beam (0.5 ps full width at half maximum (FWHM), a few electrons per pulse) with a kinetic energy of 70 keV (blue) intersects with an unknown few-cycle waveform (red) at a freestanding aluminum mirror (gray, ≈20% electron transmittance). A Ge window is used for dispersion control. Depending on their random arrival time, beam electrons are accelerated sideways by the electric field cycles of the unknown waveform. b) A time-integrating detector placed 1.3 m away from the mirror resolves a deflection histogram. Left panel, raw data; right panel, 1D profile. c) Special turning points and cutoffs (dotted lines) reveal the field cycles without the need for time resolution. Left panel, histogram of field cycles. In right panel, the reconstructed waveform (red) agrees with electro-optic sampling data (gray).

photons or bound electrons as a probe. As elementary particles in free space, beam electrons are directly and immediately accelerated in the electric field of laser light via the Lorentz force and therefore offer a linear-optical and instantaneous response to the optical waveform.[13,14,31,33,34,39–47] **Figure 1**a depicts our approach. The unknown optical waveform (red) and an electron beam (blue) interact with each other in an angled geometry in which the electric field of the waveform accelerates the electrons in a sideways direction. A modulation element (black), for example, a mirror, provides momentum and energy conservation.[14,45,48–50] The temporally long electron beam continuously covers the entire optical waveform in time, and a time-integrating detector therefore records an incoherent accumulation of deflections in form of a histogram of the field cycles. The electron beam does not have to be pulsed. It can be a continuous beam, provided that enough electrons randomly coincide in time with the optical waveform within a realistic integration time.

Mathematically, we describe the physics of free-electron deflection in a similar way as in attosecond photoelectron streaking.[51,52] When we approximate the electrons as point particles with a substantial fraction of the speed of light, the sideways deflection induced by a p-polarized plane-wave field is expressed as (see Appendix A, Supporting Information)

$$\Delta p_x\left(x, t_0\right) = eCA_{\mathrm{in}}\left(t_0 + \tau_{\mathrm{VM}}\left(x\right)\right) \tag{1}$$

where $A_{\mathrm{in}}(t)$ is the temporal part of the vector potential of the incident field, the same quantity that is obtained by photoelectron streaking.[27,28] $e$ is the elementary charge, $t_0$ is the arrival time of the electron on the foil at $x = 0$, and $\tau_{\mathrm{VM}}(x)$ is the delay due to the electron-laser velocity mismatch.[43,45] The constant $C$ is a dimensionless coupling coefficient that depends on the angles of the experiment.[43,45] Quantum-mechanically, the electrons in our beam are wave packets extended in space $x$ and time $z/v_e - t$, and the interaction with the light field is described by modulations of the phase of the de Broglie wave.[50,53–56] The quantum-coherent streaking at the mirror is

$$\Delta p_{x,\mathrm{QM}}\left(x, z - v_e t, t_0\right) = eC' A_{\mathrm{in}}\left(\frac{z}{v_e} - t + t_0 + \tau_{\mathrm{VM}}\left(x\right)\right) \tag{2}$$

where $C'$ is a dimensionless constant that is determined by the details of the streaking mechanism (see Appendix B, Supporting Information).

Both pictures show that high-energy beam electrons are deflected by the cycles of an optical waveform as a function of their arrival time in a very similar way as the bound electrons of an atom when ionized by attosecond high-energy photons under presence of an optical field.[57] However, by replacing the bound electrons with the swift free electrons in a beam, by substituting the atomic core with our macroscopic mirror membrane, we obtain an instantaneous and field-linear light–electron interaction without the need for an ultrashort probe event (i.e., attosecond ionization). The time resolution of our waveform sampling is limited only by the time it takes for a beam electron to pass though the membrane, which is less than 0.3 fs in this experiment.

## 3. Experiment and Results

In the experiment, the few-cycle laser pulses centered at 6.9 μm (50 kHz repetition rate) to be measured are produced by optical parametric amplification[58] and focused under p-polarization onto a 20 nm thick aluminum foil coated on a freestanding 20 nm thick silicon nitride membrane ($0.5 \times 0.5$ mm$^2$). The carrier-envelope phase ($\varphi_{\mathrm{CE}}$) of the few-cycle pulse is passively stable to better than 200 mrad (rms) h$^{-1}$[57] and can be shifted continuously under preservation of all other pulse parameters by simply changing the relative delay between the seed pulses and the pump pulses in our optical parametric amplifier.[8] The estimated peak field strength in the optical focus is 0.4 V nm$^{-1}$. An electron beam is generated at a kinetic energy of 70 keV and a velocity of $0.5c$ by laser-triggered photoemission and subsequent

electrostatic acceleration.[46] The diameter of the collimated electron beam (100 μm, flat top shape) is smaller than the diameter of the laser focus (≈400 μm, $1/e^2$) in order to measure a local field. The duration of the electron pulses is ≈500 fs, much longer than the optical pulses, and the entire optical waveform of interest is therefore covered with electrons at a nearly constant rate. A continuous electron beam would work as well, provided that a sufficient number of electrons randomly fall into the time range of the optical pulses within the experimental integration time.

Figure 1b depicts a typical measurement result. The direct electron beam initially hits the screen at $x = y = 0$, but in presence of the optical field, it is elongated into a line shape along the $x$-axis. This streaking direction is parallel to the electric field vector of the optical waveform, and the magnitude of deflection is directly proportional to the electromagnetic field strength (Figure S1, Supporting Information). The electrons around $x = 0$ are not helpful for waveform reconstruction (see below) and can thus be blocked. Figure 1b is deflection data in which $\varphi_{CE}$ was adjusted to give the largest deflection toward $+x$. Interestingly, the measured pattern shows several special points where there are either maximum intensities (for example, at $P_{pos}$ and $P_{neg}$) or where there are abrupt, stepwise intensity decreases (cutoffs). The dotted lines mark four such special points at −1.2, −0.6, +0.7, and +1.4 mrad. Note that the measured pattern is highly asymmetric: all cutoffs and also the four accumulation points do not have the corresponding points at opposite $x$; for example, $P_{pos}$ is at 1.2 mrad and $P_{neg}$ at −1.0 mrad. The right panel of Figure 1b shows an integration along the $y$-axis into which no streaking is induced. We see again the asymmetric peaks $P_{pos}$ and $P_{neg}$ as well as the four cutoffs of the deflection signal (dotted lines).

Given the linear relation of beam deflection to the optical waveform according to Equations (1) and (2), electrons accumulate on the detector mainly at such deflection angles where the optical waveform has a turning point, that is, an approximately constant field as a function of time. In other words, each local maximum or minimum of the waveform produces a cutoff in the streaking pattern at a deflection value given by the local peak field strength. The measured four cutoff points (dotted lines) therefore reveal that the optical waveform is a few-cycle pulse with two particular field crests in positive direction and two particular field crests in negative direction. The intensity of $P_{neg}$ is 2.1 times higher than $P_{pos}$, suggesting that $P_{neg}$ is induced by two temporally separated negative peaks of the optical waveform. We therefore conclude, so far without any numerical analysis, on a cosine-shaped waveform that consists of one positive maximum and two similar negative extrema at adjacent times. Although the precise timing of the field cycles is not yet determined, we see that the qualitative nature of an optical waveform including its carrier-envelope phase and sequence of cycles can be deduced.

In order to confirm this assessment, we plot in the right panel of Figure 1c the results of an electro-optical sampling measurement of our pulses.[8,58] In order to account for the sampling of a $A_{in}(t)$ in our experiment [see Equations (1) and (2)], we adjust the carrier-envelope phase to give a cosine-shaped waveform. The result is shown in Figure 1c as a gray line. Indeed, the optical waveform with its asymmetric shape has a complex series of field cycles at the positions and field strengths that have been deduced (dotted lines).

### 3.1. Waveform Reconstruction

A simple procedure allows to reconstruct a waveform from the experimental raw data. In most optical experiments, the spectrum $S(\omega)$ of the unknown field can be measured accurately with a spectrometer. For example, **Figure 2**e shows the spectrum of our laser pulses as obtained with Fourier-transform spectrometry. Using $S(\omega)$ and an arbitrary spectral phase $\varphi(\omega)$, the time-domain waveform can be expressed as

$$A_{in}(t) = \mathrm{Re}\left[\int_0^{+\infty} \frac{\sqrt{S(\omega)}}{\omega} e^{i\varphi(\omega)} \mathrm{d}\omega\right] \tag{3}$$

where $\omega$ is the angular frequency. Commonly, the spectral phase is Taylor-expanded around a central frequency $\omega_0$ according to

$$\varphi(\omega) = \varphi_{CE} + \varphi_{GD}(\omega - \omega_0) + \frac{\varphi_{GDD}}{2}(\omega - \omega_0)^2 + \frac{\varphi_{TOD}}{6}(\omega - \omega_0)^3 + \cdots \tag{4}$$

The waveform is then determined by the three leading parameters $\varphi_{CE}$ (the carrier-envelope phase, CEP), $\varphi_{GDD}$ (the group delay dispersion, GDD), and $\varphi_{TOD}$ (the third-order dispersion, TOD). $\varphi_{GD}$ describes a group delay and only shifts the entire waveform in time. More coefficients are typically not significant for few-cycle pulses but can be incorporated if required. We now retrieve the optical waveform from a single deflection histogram by fitting Equations (1), (3), and (4) to the measurement results. We note that a retrieval of $A_{in}(t)$ is, in principle, possible without the use of the optical spectrum, but at least $\omega_0$ has to be given in order to map the reconstructed waveform crests to timing information via the cycle period; we recall that all of our data are taken without scanning a delay time. There remains only an ambiguity in sign, to be resolved as described below.

In the measured data of Figure 1b, a cosine-like waveform has been set up in our pulse source[58] by simply maximizing the highest positive deflection ($P_{pos}$). Therefore, we assume $\varphi_{CE} = 0$ and only optimize the two remaining parameters $\varphi_{GDD}$ and $\varphi_{TOD}$ via a least square fitting algorithm to the observed deflection signal of Figure 1b. The green curve in Figure 1b and the red squares in Figure 1c show the fitting result and the retrieved field-cycle histogram, respectively. The red curve in Figure 1d shows the reconstructed waveform. We see that it is nearly identical to the waveform obtained by the electro-optical sampling reference (gray) except small details at weaker cycles. Also, the reconstructed waveform corresponds well to the direct guess of the peak amplitudes from the raw data alone (dotted lines).

### 3.2. Tomography Scans

In order to test the robustness and universality of our procedure, and to remove the time-axis ambiguity, we now scan the carrier-envelope phase ($\varphi_{CE}$) of the laser waveform and record a series of static, not-time-resolved electron deflection histograms as a function of $\varphi_{CE}$. Figure 2a shows in the left panel the raw data in the form of a series of deflection patterns (integrated along $y$). We stress again that no time delay is scanned, and each column in Figure 2a is a single time-integrated image for a particular

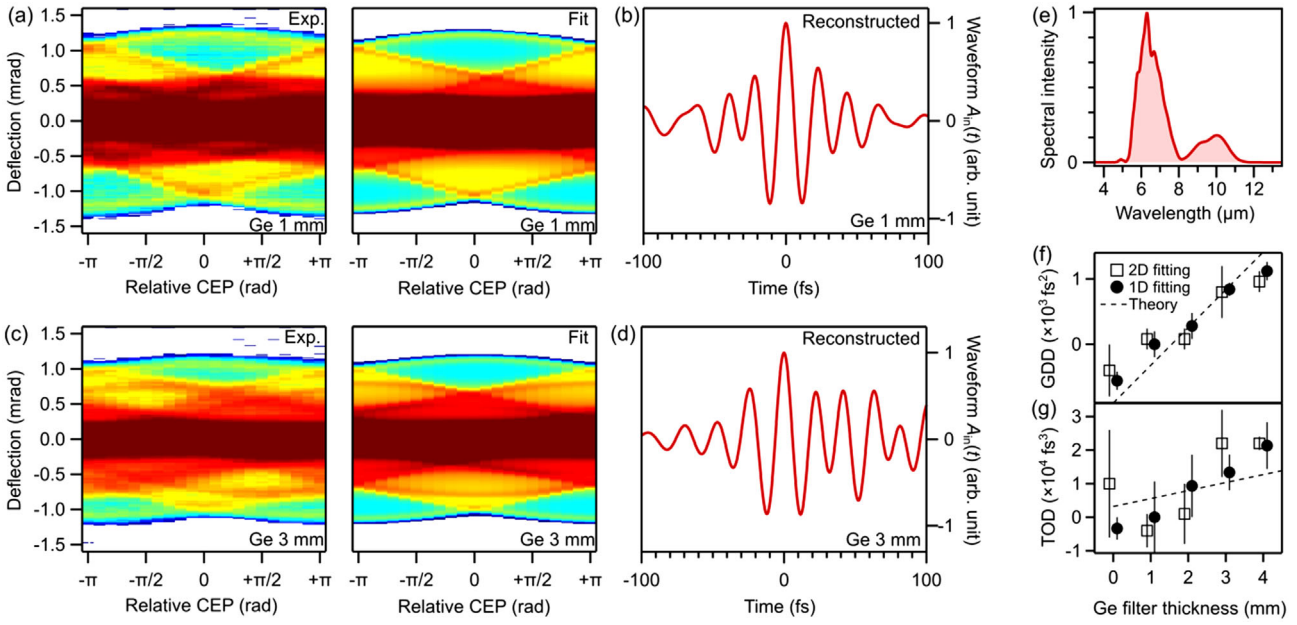


**Figure 2.** Free-electron tomography of few-cycle optical waveforms. a) Cycle tomography of an ultrashort waveform after a 1 mm thick Ge window. Color scale, see Figure 1. b) Reconstructed optical waveform. c) Cycle tomography results for dispersed pulses from a 3 mm thick Ge window. d) Reconstructed waveform. e) Measured spectrum of the single-cycle mid-infrared pulse. f) The group delay dispersion (GDD) of reconstructed waveforms as a function of material insertion. g) Third order dispersion (TOD) of the reconstructed waveforms. Dotted lines in (f) and (g) are the calculated values from the refractive index of Ge. The large error bars in the TOD data indicate that the amplitudes of the most prominent field cycles in our waveform are rather independent of a varying TOD.

$\varphi_{CE}$. We call such data a tomographic scan, because we record a series of "time-collapsed" optical waveforms under variation of $\varphi_{CE}$ in a very analogous way to X-ray tomography, where one accumulates a series of "depth-collapsed" projection images under variation of an illumination angle. In Figure 2a, we see several curved lines (e.g., dark blue, orange, red, dark red) with complex near-sinusoidal shapes as a function of $\varphi_{CE}$. These changes of cutoffs and peaks correspond to gradually changing field strengths of the different optical cycles. Deflection signals at $\varphi_{CE} = \pm\pi$ are nearly identical with those at $\varphi_{CE} = 0$ when flipped upside down, as expected from the change of a cosine-shaped to a minus-cosine-shaped waveform. The extreme cutoffs at maximum positive and negative deflections (dark blue) go in parallel, indicating the simultaneous loss and gain of the highest positive and lowest negative waveform crest as a function of $\varphi_{CE}$. Figure 2c shows such a scan for the case of an intentionally chirped optical waveform. We now see more peaks and fringes, as expected from the multiple field cycles that are now involved. Also, the dependency on $\varphi_{CE}$ becomes more complex than that without the chirp. In particular, the result becomes sensitive to time reversal.

For analyzing such tomographic scans, we simply optimize the three parameters $\varphi_{CE}$, $\varphi_{GDD}$, and $\varphi_{TOD}$ with a global fit. The right panel of Figure 2a shows the simulated tomography signal and Figure 2b depicts the reconstructed waveform. All the features are well reproduced. The reconstruction of the chirped pulse data of Figure 2c is depicted in Figure 2d. Also, here, the tomography image is well reproduced, and the reconstructed waveform now reveals an asymmetric shape in time due to the influences of third-order dispersion.

### 3.3. Consistency Checks with Dispersion Control

In another experiment, we record electron beam deflection data as a function of a varying dispersion of the optical waveform, produced by introducing four different germanium windows into the optical beam path. Each time, we record a single waveform shadow at $\varphi_{CE} = 0$ like in Figure 1a and then evaluate the optical waveform according to Equation (4). The black circles in Figure 2f,g show the obtained GDD ($\varphi_{GDD}$) and TOD ($\varphi_{TOD}$), respectively. When using a complete tomography scan under variation of $\varphi_{CE}$ for all four dispersions, followed by four global fits, we obtain the black open squares. Both analyses provide nearly the same results. All measured dispersion values scale approximately linear with the window thickness and the slopes are consistent with the literature values[59] (dotted lines).

The general similarity of all experimental and simulation data in Figure 2a,c in combination with the agreement to electro-optical sampling and recorded dispersion data establish the accuracy of free-electron tomography to capture electromagnetic few-cycle waveforms of almost arbitrary shape. Essentially, we require neither a nonlinear optical process nor an ultrashort probe event.

## 4. Multidimensional Space-Time Tomography with Electron Microscopy

**Figure 3**a depicts a proof-of-concept experiment for a combination of the above reported free-electron tomography with transmission electron microscopy. The spatiotemporal optical waveform to be determined is guided onto a large mirror membrane (gray) under an incidence angle of 45° in the *xy*-plane with help

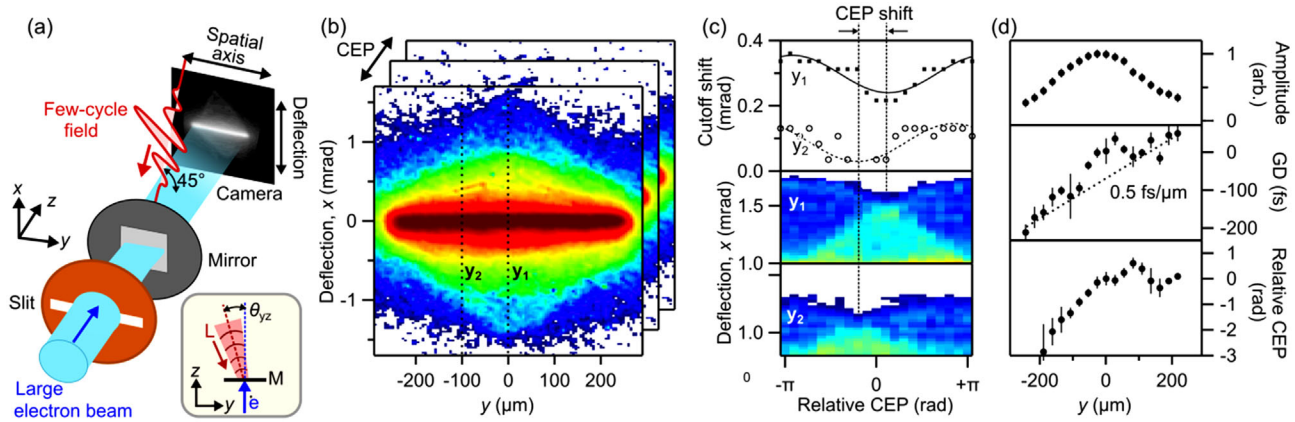


**Figure 3.** Electron microscopy combined with waveform tomography. a) Experimental setup. A collimated electron beam (blue) passes through a slit ($100 \times 2000$ μm$^2$, orange) and specimen (gray) that is illuminated by a p-polarized few-cycle field (red) at 45° incidence angle in $x$–$z$-plane and a small angle $\theta_{yz}$ in the $y$–$z$-plane. The optical polarization is in the $xz$-plane. Quadrupole lenses (not depicted) provide a magnified image along $y$ (5.4 μm per pixel). Inset, top view of the $y$–$z$-plane. M, mirror; L, laser beam. b) Observed images on the screen. Color scale, see Figure 1. c) Analysis of tomography lines and cutoffs. Top panel, shift of cutoff angles at $y_1 = 0$ μm (squares) and $y_2 = -100$ μm (open dots). Curves show fit results. Middle and lower panels, tomography signals around these cutoff angles. Color scale, see Figure 1 at one tenth of the range. d) Evaluated waveform amplitudes, group delays and CEPs as a function of the $y$-coordinate.

of a parabolic mirror. The laser focus is set to about 3 mm behind the crossing point with the electron beam in order to produce a nontrivial waveform in space and time. A large-diameter electron beam is converted into a nearly linear shape with help of a slit aperture (orange). Consequently, our detector screen measures time-integrated free-electron streaking along the $x$-axis that is spatially resolved as a function of the position along the $y$-axis. Postspecimen quadrupole magnets (not depicted) provide special resolution along the $y$-axis while maintaining angular resolution in the streaking direction along $x$.

As illustrated in Figure 3b, we observed a series of 2D tomography images as a function of $\varphi_{CE}$. Again, no ultrashort probe event is applied, and no delay time is scanned. For each $y$ (horizontal direction), a waveform is reconstructed as demonstrated above. Figure 3c shows in the two lower panels the measured tomographic signals as a function of $\varphi_{CE}$ for two example positions $y_1$ and $y_2$. We see at least two special lines (dark blue and turquoise) with sinusoidal dependencies on $\varphi_{CE}$, but their minima and maxima are shifted substantially; see the upper panel of Figure 3c. This observation is direct evidence for a change of the carrier-envelope phase as a function of position along $y$.

Each tomography dataset produces values for the overall waveform amplitude and the spectral phases of Equations (3) and (4) as a function of the position $y$. Because $\varphi_{GD}$ can never be revealed in our non-time-resolved experiment, we determine it with a scan of the macroscopic electron-laser delay at a fixed CEP and subsequent search for the maximum deflection angles. This measurement is the only data in this report where a time delay is scanned. Figure 3d shows the combined results. The upper panel shows the absolute field amplitude of the waveform. It reveals a Gaussian function that corresponds to the optical beam profile. The middle panel shows the group delay of the optical field. We see a nearly linear increase (dotted line) and a slight curvature at the beam center. The slope of 0.5 fs μm$^{-1}$ reveals that the laser pulses travel on the mirror surface at a surface speed of 2 μm fs$^{-1}$ or 6.7$c$, indicating an incidence angle of $\theta_{yz} = 9°$ in the $yz$-plane; see inset of Figure 3a. The curvature of the group delay at the beam center is attributed to the curved wave front of a converging beam outside the focus; see inset of Figure 3a. The dispersions $\varphi_{GDD}$ and $\varphi_{TOD}$ are not substantially changing as a function of $y$ (see Appendix D, Supporting Information). However, the lower panel in Figure 3d shows the carrier-envelope phase $\varphi_{CE}$ as a function of $y$. We see a change of $\approx\pi$ over the beam size and also a substantial curvature. These observations are incompatible with the Gouy phase shifts of a perfect monochromatic Gaussian beam and demonstrate the presence and significance of the focal phases[60,61] of realistic few-cycle fields that are, for example, essential for strong-field experiments.[62] More experimental results on few-cycle waveforms before, at, and after the nominal focus position are reported in Appendix D, Supporting Information.

## 5. Sensitivity

We assess the generality and applicability of our method to weak and special waveforms. In principle, there are two aspects of resolution that are related. On the one hand, the deflection caused by the optical waveform must exceed the intrinsic divergence angle of the electron beam. This divergence is limited by the source brightness and the size of the optical focus. On the other hand, a minimum accumulated amount of electrons must coincide with each optical cycle in the time domain to make it visible in the data. This coverage is limited by the electron beam current. Together, we see that the brightness of the electron source is the essential factor for our waveform tomography.

How many electrons are needed? We estimate from simulations that at least a number of $N_e \approx 100$ electrons must fall into each optical cycle. With an average current $I$ of the electron beam, a waveform repetition rate $\nu$, and the center frequency $\omega_0$ of the optical cycles, the needed experimental integration time $T_{tot}$ becomes $T_{tot} \approx \frac{N_e \omega_0 e}{2\pi I \nu}$. For example, a continuous electron beam

in a transmission electron microscope has a typical current of $I \approx 10$ nA. Assuming a laser repetition rate of $\nu = 100$ kHz and a center frequency of $\omega_0 = 273$ THz at 6.9 μm wavelength, the total integration time becomes $T_{\text{tot}} \approx 0.7$ s per deflection histogram, eventually to be multiplied by the needed numbers of parameters for a complete tomography, if desired. We see that the ability of our cycle tomography to measure optical waveforms is not restricted to pulsed electron sources and can work with a continuous electron beam as well.

Assuming enough electrons, we now ask, how long optical pulses can still be measured appropriately? In too long pulses, adjacent cycles will produce an indistinguishable deflection and the histogram will smear out beyond the point of cycle-based information. Mirror membranes can produce a deflection angle of approximately up to[45] $\alpha_{\text{deflect}} \approx \frac{e}{m_e} \frac{\lambda_L}{2\pi c} \frac{1}{v_e} E_0$, where $E_0$ is the electric field amplitude and $\lambda_L$ is the central wavelength of the optical field. In order to distinguish a certain field cycle from an adjacent one, this deflection should be different enough. Assuming a Fourier-transform-limited pulse of a duration $\tau_{\text{FWHM}}$, the deflection angle by the second-strongest peak is $\alpha_{\text{deflect,2nd}} = \alpha_{\text{deflect}} \exp(-2\ln(2)(\frac{\lambda_L}{c\tau_{\text{FWHM}}})^2)$. The two cycles can be distinguished if the two deflection signals $\alpha_{\text{deflect}}$ and $\alpha_{\text{deflect,2nd}}$ are well separated with respect to $\alpha_{\text{beam}}$, the intrinsic divergence of the electron beam, that is, $\alpha_{\text{deflect}} - \alpha_{\text{deflect,2nd}} > \alpha_{\text{beam}}$. We see that only the quality of the electron beam limits the achievable dynamic range of pulses to be determined. For the conditions of the experiment ($\alpha_{\text{beam}} \approx 0.1$ mrad, $E_0 = 0.4$ V nm$^{-1}$, $\lambda_L = 6.9$ μm), we obtain $\tau_{\text{FWHM}} < 130$ fs (≈5.6 cycles). For a near-infrared femtosecond source with $\lambda_L = 780$ nm and $E_0 = 3$ V nm$^{-1}$ (≈$10^{12}$ W cm$^{-2}$),[63] we obtain $\tau_{\text{FWHM}} < 14$ fs (≈5.4 cycles). The limiting factor is solely the emittance of the electron beam, which can be made 100–1000 times better than in our experiment,[64] if required.

Assuming a single-cycle waveform, how weak fields can still be detected? The angle $\alpha_{\text{deflect}}$ must be larger than the intrinsic angle spread $\alpha_{\text{beam}}$. Using an electron beam with an emittance $\varepsilon$ focused down to a diameter of $\sim \lambda_L$, we obtain $\alpha_{\text{beam}} = \varepsilon/\lambda_L$. Setting $\alpha_{\text{deflect}} = \alpha_{\text{beam}}$ and assuming an electron beam[64] with $\varepsilon \approx 2$ pm rad$^{-1}$ at $v_e \approx 0.5c$, we obtain $E \approx 10^5$ V m$^{-1}$. Such values are not too far away from the typical electric field strength of thermal radiation (see Appendix E, Supporting Information) or vacuum fluctuations[65] and correspond to optical pulses with merely femtojoule of pulse energy, the same or less than in recent results with the on-chip waveform sampling.[36] In principle, the emittance of an electron beam for tomography purposes can be almost arbitrarily improved with apertures or other filters at cost of electron flux, so further advancements can be conceived. For example, it should be possible to assess electric-field fluctuations or squeezing by observing correlations in the deflection data on basis of detecting single-electron events.

In many high-field experiments with short laser pulses, it is essential to know the amount of pulse energy that is within the main peak in comparison to a background-like intensity around it. Our waveform tomography could be well suited to measure this ratio simply by relating the total amount of deflected electrons above a certain angle (defined by the definition of pulse width) with respect to all other electrons that are deflected less. In the experiment, we have resolved the intrinsic time ambiguity of a single deflection histogram by rotating the CEP by $2\pi$, but any other controllable laser parameter that breaks the temporal symmetry of the optical cycles will be useful as well. The theoretical framework of Section 2 and appendices A and B allow to predict the achievable level of sensitivity for a given question and set of laser parameters in a rather straightforward way. If the experiment is repeated on a single-shot/single-electron basis, we will also become sensitive to fluctuations and classical or nonclassical statistics of the optical field with subcycle time resolution.

## 6. Conclusion and Outlook

The concept and experimental results reported in this work establish the ability to measure optical waveforms without the need for either a nonlinear-optical phenomenon or an ultrafast time resolution. The origin of this capability is the elementary charge of the electron and its large velocity in a free-space beam. High-energy beam electrons can be focused down to sub-nanometer dimensions and a transmission electron microscope without particular time resolution is therefore useful for measuring electromagnetic waveforms of almost any optical wavelength in space and time. The reported unification of few-cycle laser science with free-space electron beams and non-time-resolved electron microscopy may therefore open up novel research directions in the fields of nanophotonics, metamaterials, nonlinear optics, high-field physics, free-electron quantum optics, dielectric particle acceleration, and many more.

## Supporting Information

Supporting Information is available from the Wiley Online Library or from the author.

## Acknowledgements

The authors thank Simon Stork for help with mirror preparation and Ferenc Krausz for laboratory infrastructure. Y.M. acknowledges Peter Hommelhoff for general support. The authors acknowledge funding from the German Science Foundation via SFB 1432, the Dr. K. H. Eberle Stiftung, the Vector Stiftung, and the FAU Emerging Talent Initiative.

Open access funding enabled and organized by Projekt DEAL.

## Conflict of Interest

The authors declare no conflict of interest.

## Data Availability Statement

All relevant data are available from the corresponding authors upon reasonable request.

## Keywords

attosecond physics, ultrafast electron microscopy, ultrashort laser pulses

Received: April 28, 2022
Revised: July 18, 2022
Published online:

[1] M. Ossiander, F. Siegrist, V. Shirvanyan, R. Pazourek, A. Sommer, T. Latka, A. Guggenmos, S. Nagele, J. Feist, J. Burgdörfer, R. Kienberger, M. Schultze, *Nat. Phys.* **2017**, *13*, 280.
[2] S. Grundmann, D. Trabert, K. Fehre, N. Strenger, A. Pier, L. Kaiser, M. Kircher, M. Weller, S. Eckart, L. P. H. Schmidt, F. Trinter, T. Jahnke, M. S. Schöffler, R. Dörner, *Science* **2020**, *370*, 339.
[3] M. F. Kling, C. H. Siedschlag, A. J. Verhoef, J. I. Khan, M. Schultze, T. H. Uphues, Y. Ni, M. Uiberacker, M. Drescher, F. Krausz, M. J. J. Vrakking, *Science* **2006**, *312*, 246.
[4] G. G. Paulus, F. Grasbon, H. Walther, P. Villoresi, M. Nisoli, S. Stagira, E. Priori, S. De Silvestri, *Nature* **2001**, *414*, 182.
[5] C. A. Haworth, L. E. Chipperfield, J. S. Robinson, P. L. Knight, J. P. Marangos, J. W. G. Tisch, *Nat. Phys.* **2007**, *3*, 52.
[6] O. Schubert, M. Hohenleutner, F. Langer, B. Urbanek, C. Lange, U. Huttner, D. Golde, T. Meier, M. Kira, S. W. Koch, R. Huber, *Nat. Photonics* **2014**, *8*, 119.
[7] T. T. Luu, M. Garg, S. Y. Kruchinin, A. Moulet, M. T. Hassan, E. Goulielmakis, *Nature* **2015**, *521*, 498.
[8] Y. Morimoto, Y. Shinohara, M. Tani, B.-H. Chen, K. L. Ishikawa, P. Baum, *Optica* **2021**, *8*, 382.
[9] B. Xue, Y. Tamaru, Y. Fu, H. Yuan, P. Lan, O. D. Mücke, A. Suda, K. Midorikawa, E. J. Takahashi, *Sci. Adv.* **2020**, *6*, eaay2802.
[10] M. Krüger, M. Schenk, P. Hommelhoff, *Nature* **2011**, *475*, 78.
[11] G. Herink, D. R. Solli, M. Gulde, C. Ropers, *Nature* **2012**, *483*, 190.
[12] B. Piglosiewicz, S. Schmidt, D. J. Park, J. Vogelsang, P. Groß, C. Manzoni, P. Farinello, G. Cerullo, C. Lienau, *Nat. Photonics* **2014**, *8*, 37.
[13] Y. Morimoto, P. Baum, *Nat. Phys.* **2018**, *14*, 252.
[14] Y. Morimoto, P. Baum, *Phys. Rev. Lett.* **2020**, *125*, 193202.
[15] A. Schiffrin, T. Paasch-Colberg, N. Karpowicz, V. Apalkov, D. Gerster, S. Mühlbrandt, M. Korbman, J. Reichert, M. Schultze, S. Holzner, J. V. Barth, R. Kienberger, R. Ernstorfer, V. S. Yakovlev, M. I. Stockman, F. Krausz, *Nature* **2013**, *493*, 70.
[16] T. Rybka, M. Ludwig, M. F. Schmalz, V. Knittel, D. Brida, A. Leitenstorfer, *Nat. Photonics* **2016**, *10*, 667.
[17] T. Higuchi, C. Heide, K. Ullmann, H. B. Weber, P. Hommelhoff, *Nature* **2017**, *550*, 224.
[18] K. Schmid, L. Veisz, F. Tavella, S. Benavides, R. Tautz, D. Herrmann, A. Buck, B. Hidding, A. Marcinkevicius, U. Schramm, M. Geissler, J. Meyer-ter-Vehn, D. Habs, F. Krausz, *Phys. Rev. Lett.* **2009**, *102*, 124801.
[19] M. Ouillé, A. Vernier, F. Böhle, M. Bocoum, A. Jullien, M. Lozano, J.-P. Rousseau, Z. Cheng, D. Gustas, A. Blumenstein, P. Simon, S. Haessler, J. Faure, T. Nagy, R. Lopez-Martens, *Light: Sci. Appl.* **2020**, *9*, 47.
[20] J. A. Armstrong, *Appl. Phys. Lett.* **1967**, *10*, 16.
[21] R. Trebino, D. J. Kane, *J. Opt. Soc. Am. A* **1993**, *10*, 1101.
[22] P. O'Shea, M. Kimmel, X. Gu, R. Trebino, *Opt. Lett.* **2001**, *26*, 932.
[23] C. Iaconis, I. A. Walmsley, *Opt. Lett.* **1998**, *23*, 792.
[24] M. Miranda, C. L. Arnold, T. Fordell, F. Silva, B. Alonso, R. Weigand, A. L'Huillier, H. Crespo, *Opt. Express* **2012**, *20*, 18732.
[25] Q. Wu, X.-C. Zhang, *Appl. Phys. Lett.* **1995**, *67*, 3523.
[26] A. Leitenstorfer, S. Hunsche, J. Shah, M. C. Nuss, W. H. Knox, *Appl. Phys. Lett.* **1999**, *74*, 1516.
[27] E. Goulielmakis, *Science* **2004**, *305*, 1267.
[28] A. Korobenko, K. Johnston, M. Kubullek, L. Arissian, Z. Dube, T. Wang, M. Kübel, A. Y. Naumov, D. M. Villeneuve, M. F. Kling, P. B. Corkum, A. Staudte, B. Bergues, *Optica* **2020**, *7*, 1372.
[29] K. T. Kim, C. Zhang, A. D. Shiner, B. E. Schmidt, F. Légaré, D. M. Villeneuve, P. B. Corkum, *Nat. Photonics* **2013**, *7*, 958.
[30] C. Kealhofer, W. Schneider, D. Ehberger, A. Ryabov, F. Krausz, P. Baum, *Science* **2016**, *352*, 429.
[31] D. Zhang, A. Fallahi, M. Hemmer, X. Wu, M. Fakhari, Y. Hua, H. Cankaya, A.-L. Calendron, L. E. Zapata, N. H. Matlis, F. X. Kärtner, *Nat. Photonics* **2018**, *12*, 336.
[32] I. H. Baek, H. W. Kim, H. S. Bark, K.-H. Jang, S. Park, J. Shin, Y. C. Kim, M. Kim, K. Y. Oang, K. Lee, F. Rotermund, N. A. Vinokurov, Y. U. Jeong, *Nat. Commun.* **2021**, *12*, 6851.
[33] E. C. Snively, M. A. K. Othman, M. Kozina, B. K. Ofori-Okai, S. P. Weathersby, S. Park, X. Shen, X. J. Wang, M. C. Hoffmann, R. K. Li, E. A. Nanni, *Phys. Rev. Lett.* **2020**, *124*, 054801.
[34] F. Qi, Z. Ma, L. Zhao, Y. Cheng, W. Jiang, C. Lu, T. Jiang, D. Qian, Z. Wang, W. Zhang, P. Zhu, X. Zou, W. Wan, D. Xiang, J. Zhang, *Phys. Rev. Lett.* **2020**, *124*, 134803.
[35] S. Sederberg, D. Zimin, S. Keiber, F. Siegrist, M. S. Wismer, V. S. Yakovlev, I. Floss, C. Lemell, J. Burgdörfer, M. Schultze, F. Krausz, N. Karpowicz, *Nat. Commun.* **2020**, *11*, 430.
[36] M. R. Bionta, F. Ritzkowsky, M. Turchetti, Y. Yang, D. Cattozzo Mor, W. P. Putnam, F. X. Kärtner, K. K. Berggren, P. D. Keathley, *Nat. Photonics* **2021**, *15*, 456.
[37] N. K. Berger, B. Levit, V. Smulakovsky, B. Fischer, *Appl. Opt.* **2005**, *44*, 7862.
[38] A. Borzsonyi, A. Kovacs, K. Osvay, *Appl. Sci.* **2013**, *3*, 515.
[39] L. Zhao, Z. Wang, C. Lu, R. Wang, C. Hu, P. Wang, J. Qi, T. Jiang, S. Liu, Z. Ma, F. Qi, P. Zhu, Y. Cheng, Z. Shi, Y. Shi, W. Song, X. Zhu, J. Shi, Y. Wang, L. Yan, L. Zhu, D. Xiang, J. Zhang, *Phys. Rev. X* **2018**, *8*, 021061.
[40] L. Zhao, H. Tang, C. Lu, T. Jiang, P. Zhu, L. Hu, W. Song, H. Wang, J. Qiu, C. Jing, S. Antipov, D. Xiang, J. Zhang, *Phys. Rev. Lett.* **2020**, *124*, 054802.
[41] H. W. Kim, N. A. Vinokurov, I. H. Baek, K. Y. Oang, M. H. Kim, Y. C. Kim, K.-H. Jang, K. Lee, S. H. Park, S. Park, J. Shin, J. Kim, F. Rotermund, S. Cho, T. Feurer, Y. U. Jeong, *Nat. Photonics* **2020**, *14*, 245.
[42] L. Zhao, Z. Wang, H. Tang, R. Wang, Y. Cheng, C. Lu, T. Jiang, P. Zhu, L. Hu, W. Song, H. Wang, J. Qiu, R. Kostin, C. Jing, S. Antipov, P. Wang, J. Qi, Y. Cheng, D. Xiang, J. Zhang, *Phys. Rev. Lett.* **2019**, *122*, 144801.
[43] Y. Morimoto, P. Baum, *Phys. Rev. A* **2018**, *97*, 033815.
[44] D. S. Black, U. Niedermayer, Y. Miao, Z. Zhao, O. Solgaard, R. L. Byer, K. J. Leedle, *Phys. Rev. Lett.* **2019**, *123*, 264802.
[45] D. Ehberger, A. Ryabov, P. Baum, *Phys. Rev. Lett.* **2018**, *121*, 094801.
[46] D. Ehberger, K. J. Mohler, T. Vasileiadis, R. Ernstorfer, L. Waldecker, P. Baum, *Phys. Rev. Appl.* **2019**, *11*, 024034.
[47] J. D. Jackson, *Classical Electrodynamics*, John Wiley & Sons, Inc., New York **1999**.
[48] T. Plettner, R. L. Byer, E. Colby, B. Cowan, C. M. S. Sears, J. E. Spencer, R. H. Siemann, *Phys. Rev. Lett.* **2005**, *95*, 134801.
[49] F. O. Kirchner, A. Gliserin, F. Krausz, P. Baum, *Nat. Photonics* **2014**, *8*, 52.
[50] G. M. Vanacore, I. Madan, G. Berruto, K. Wang, E. Pomarico, R. J. Lamb, D. McGrouther, I. Kaminer, B. Barwick, F. J. García de Abajo, F. Carbone, *Nat. Commun.* **2018**, *9*, 2694.
[51] J. Itatani, F. Quéré, G. L. Yudin, M. Y. Ivanov, F. Krausz, P. B. Corkum, *Phys. Rev. Lett.* **2002**, *88*, 173903.
[52] M. Kitzler, N. Milosevic, A. Scrinzi, F. Krausz, T. Brabec, *Phys. Rev. Lett.* **2002**, *88*, 173904.
[53] L. S. Brown, T. W. B. Kibble, *Phys. Rev.* **1964**, *133*, A705.
[54] S. T. Park, M. Lin, A. H. Zewail, *New J. Phys.* **2010**, *12*, 123028.
[55] Y. Morimoto, P. Hommelhoff, *Phys. Rev. Res.* **2020**, *2*, 043089.
[56] A. Feist, S. V. Yalunin, S. Schäfer, C. Ropers, *Phys. Rev. Res.* **2020**, *2*, 043227.
[57] M. Hentschel, R. Kienberger, C. Spielmann, G. A. Reider, N. Milosevic, T. Brabec, P. Corkum, U. Heinzmann, M. Drescher, F. Krausz, *Nature* **2001**, *414*, 509.
[58] B.-H. Chen, E. Wittmann, Y. Morimoto, P. Baum, E. Riedle, *Opt. Express* **2019**, *27*, 21306.

[59] H. H. Li, *J. Phys. Chem. Ref. Data* **1980**, *9*, 561.
[60] F. Lindner, G. G. Paulus, H. Walther, A. Baltuška, E. Goulielmakis, M. Lezius, F. Krausz, *Phys. Rev. Lett.* **2004**, *92*, 113001.
[61] D. Hoff, M. Krüger, L. Maisenbacher, A. M. Sayler, G. G. Paulus, P. Hommelhoff, *Nat. Phys.* **2017**, *13*, 947.
[62] Y. Zhang, D. Zille, D. Hoff, P. Wustelt, D. Würzler, M. Möller, A. M. Sayler, G. G. Paulus, *Phys. Rev. Lett.* **2020**, *124*, 133202.
[63] M. Schultze, K. Ramasesha, C. D. Pemmaraju, S. A. Sato, D. Whitmore, A. Gandman, J. S. Prell, L. J. Borja, D. Prendergast, K. Yabana, D. M. Neumark, S. R. Leone, *Science* **2014**, *346*, 1348.
[64] A. Feist, N. Bach, N. Rubiano da Silva, T. Danz, M. Möller, K. E. Priebe, T. Domröse, J. G. Gatzmann, S. Rost, J. Schauss, S. Strauch, R. Bormann, M. Sivis, S. Schäfer, C. Ropers, *Ultramicroscopy* **2017**, *176*, 63.
[65] C. Riek, D. V. Seletskiy, A. S. Moskalenko, J. F. Schmidt, P. Krauspe, S. Eckart, S. Eggert, G. Burkard, A. Leitenstorfer, *Science* **2015**, *350*, 420.